A new, sustainable LaFeO3 material prepared from biowaste-sourced soluble substances

Journal Name

Dynamic Article Links ►

Cite this: DOI: 10.1039/c0xx00000x

www.rsc.org/xxxxxx

ARTICLE TYPE

A new sustainable $LaFeO_3$ material prepared from biowaste sourced soluble substances

Francesca Deganello,*[a] Maria LauraTummino,[a,b] Carla Calabrese,[a] Maria Luisa Testa,[a] Paola Avetta,[b] Debora Fabbri,[b] Alessandra Bianco Prevot,[b] Enzo Montoneri[c] and Giuliana Magnacca[b,d]

Received (in XXX, XXX) Xth XXXXXXXXX 20XX, Accepted Xth XXXXXXXXX 20XX

DOI: 10.1039/b000000x

For the first time, sustainable $LaFeO_3$ powders were prepared from soluble bio-based substances (SBO) extracted from urban wastes. For the preparation of the perovskite-type powders, a modified solution combustion synthesis route was used, where SBO have the triple role of fuel, complexant and microstructural template. A careful examination of the $LaFeO_3$ powders, by using complementary characterization techniques, evidenced their peculiar microstructural, morphological, textural and photocatalytic properties. Preliminary photodegradation tests of a phenol-based wastewater pollutant and photobleaching of a model-dye were performed on the waste-derived $LaFeO_3$ powders; the obtained results encourage further studies on the application of these materials as heterogeneous catalysts for wastewater treatment. Moreover, a meaningful amount of entrapped matter was evidenced in the powders, which is responsible of most of their peculiar properties.

Introduction

Environmental protection is worldwide considered a primary issue of the sustainable development.[1] In order to preserve our environment, scientific research has been recently moved towards two main directions: the recycle and reuse of wastes, which represent a never-ending resource, and the depollution of air, waters and soils. A major challenge is of course to remedy the polluted environment by re-using wastes. New eco-friendly materials manufacture methods, where renewable sources are efficiently used for energy production and environmental protection, have been recently developed in the literature.[2]

$LaFeO_3$ mixed oxides with ABO_3 perovskite-type structure are becoming more and more important because of their catalytic and electrical properties that make them suited as sensors, oxidation catalysts for air pollutants, fuel cells electrodes and oxygen permeation membranes.[3,4] Moreover, $LaFeO_3$ are well known photocatalysts and they have already been tested for the abatement of various pollutants.[5-9] Photocatalysis is a procedure included in the broader field of the advanced oxidation processes (AOPs), designed to remove organic materials in wastewaters, through the formation of reactive oxygen species.[10-13] Among many candidates for photocatalysis,[14] TiO_2 shows very efficient photoactivity under UV-light irradiation (TiO_2 band gap is about 3 eV).[15] On the other hand, the advantage of using $LaFeO_3$ powders, as it or supported,[16,17] is their activation by visible light, thanks to the smaller band gap (about 2.1 eV).[3,18]

In order to obtain a controlled microstructure, $LaFeO_3$ synthesis has been carried out with several templating agents like dioctylsulfosuccinate sodium,[19] carbon nanotubes, [20] mesoporous silica (SBA-16),[9] hexadecyltrimethyl ammonium bromide,[21] porous anodic aluminum oxide,[22] polyoxyethylene(5)nonylphenylether[23] and polystyrene,[24] some of which have as well surfactant properties.[19,21]

In this work, the production of a $LaFeO_3$ powder to be tested as photocatalyst is carried out for the first time through a modified solution combustion synthesis (SCS) route in the presence of soluble bio-based substances (SBO) extracted from urban wastes.

The SBO have been reported constituted by a mix of polymeric molecules containing a variety of C types and functional groups of different polarity.[25] These chemical features have been shown to be responsible of their surfactant properties; *i.e.* in water solution they yield pseudomicelles and/or large molecular aggregates. For these properties they have been successfully employed in substitution of synthetic surfactants as auxiliaries in formulations for textile dyeing,[26] detergency[26] and environmental decontamination processes,[27] as well as microstructural bio-templates for the preparation of iron-doped hydroxyapatite,[28] SiO_2[29] and TiO_2[30] nanopowders. The SBO have been also employed as photosensitizers[31-33] and adsorption-promoting materials.[34] The SCS process shows high similarities with the very well-known Pechini process and it can be also described as a “sol–gel combustion method”. Nevertheless, this method differs from Pechini process in that the nitrates are not previously eliminated as NOx, but react with the fuel to start a heat-induced chemical chain reaction.[35]

The present work shows that the SBO have the triple role of fuel, chelating agents and microstructural bio-templates. It proves also that SBO micelles act as a pattern on which, after burning,

$LaFeO_3$ with a porous structure is formed. The product has been characterized and tested as heterogeneous photocatalysts for the degradation of 4-methyl phenol (4-MP) and of hexamethyl-*p*-rosaniline chloride (Crystal Violet, CV).

Materials and methods

SBO extraction and characterization

In the present study, SBO indicates substances extracted from biomass (supplied by ACEA Pinerolese S.p.a., Italy), consisting, in this particular case, in the green fraction of refuse, treated with aerobic digestion for 230 days (CVT230).[32] Once isolated, CVT230 was characterized according to a previously reported procedure.[36] Table 1 reports the obtained chemical data, while Fig.1 represents a virtual molecular fragment fitting the analytical data.

Table 1 CVT230 functional groups distribution. Percentage of organic moieties and/or functional groups are expressed as amount of C over total C. Metals concentration determined in the CVT230 inorganic residue, expressed as % w/w.

Aliphatic C	O-Me + N-R	O-R	Anomeric C
29.05	5.96	20.18	6.73
Aromatic C	**PhOH + PHO⁻**	**COOX (X = OH, N)**	**Keto C**
16.03	8.17	11.75	2.13

Si	Fe	Al	Mg
2.55 ± 0.01	0.77 ± 0.04	0.49 ± 0.04	1.13 ± 0.06

Ca	K	Na
6.07 ± 0.38	3.59 ± 0.21	0.16 ± 0.01

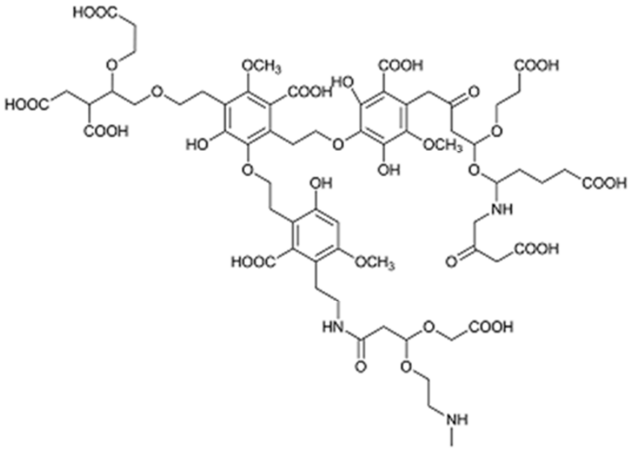

Fig. 1 Virtual molecular fragment of CVT230 molecule fitting analytical data.

The metal content of the CVT230 inorganic residue, after calcination in muffle furnace, was determined by ICP analysis. Metal cations concentration is also reported in Table 1.

Powder preparation

Preparation of the perovskite-type powders was carried out according to Scheme 1. 3.567 g of $La(NO_3)_3{\cdot}6H_2O$ (≥99.999%, Aldrich) and 3.328 g of $Fe(NO_3)_3{\cdot}9H_2O$ (≥99.99, Aldrich) were dissolved together in a minimum amount of distilled water (600 mL) to get a clear solution. A proper amount of CVT230 (CVT230/metal nitrates ratio=0.1) was then added to the metal precursors solution, in order to reach, after dilution, its critical micellar concentration (CMC), which is 2.1 g L^{-1}.[27] Ammonium nitrate (99% Sigma Aldrich) was added to regulate the reducers-to-oxidizers ratio (Φ), which was calculated taking into account the model molecular unit of Fig.1. Finally, ammonia solution (~28 wt.%, Fluka) was slowly added to adjust the pH at 6. In a 5 L beaker, in contact with a hot plate, the water solution was left to evaporate at 80° C with continuous mechanical stirring, until a sticky brown gel was obtained. In order to carry out the gel decomposition under controlled conditions, the hot plate temperature was then set to 300° C to decompose the gel by self-ignition. For the sake of comparison, a $LaFeO_3$ and a 20% Ca-doped $LaFeO_3$ were also prepared following the classical procedure with citric acid (ultrapure, Fluka) as a combustion fuel.[35] In the case of Ca-doped material $CaCO_3$ was added as a Ca precursor.

The as-burned powders were then fired in static air at 700°C for 5 h, unless otherwise specified. About 2 g of perovskite were obtained from each synthesis. In the following discussion, $LaFeO_3$ prepared from citric acid will be referred as LF, Ca-doped $LaFeO_3$ will be indicated as LF-Ca, whereas $LaFeO_3$ prepared from CVT230 will be named after LF-B.

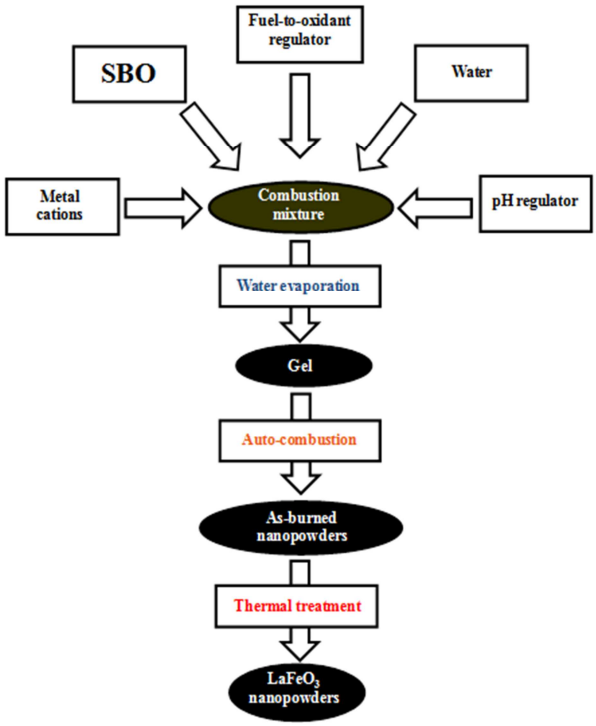

Scheme 1 Schematic description of the solution combustion synthesis adopted for the preparation of $LaFeO_3$ powders from SBO.

Physicochemical characterization

The temperature profile of the reaction medium was recorded during the combustion process by means of a K-type thermocouple (1.5 mm in diameter) coupled with a data logger (PICO technology) with a sampling velocity of 20 bit/sec and a computer with Picolog software.

X-ray diffraction (XRD) measurements were carried out on a Bruker-Siemens D5000 X-ray powder diffractometer equipped with a Kristalloflex 760 X-ray generator and with a curved graphite monochromator using the Cu Kα radiation (40 kV/30 mA). The 2θ step size was 0.03°. The integration time was 3 s per step, and the 2θ scan ranged from 10° to 90°. The diffraction patterns were analyzed by Rietveld refinement using the GSAS package.[37,38] Chebyschev polynomials functions were chosen for the background and for the peak profile fitting, respectively. In the structure refinement lattice constants, Debye Waller factors, microstrain and full width half maximum (FWHM) were considered as variables parameters. From fitting results, the structural parameters of the investigated compounds and, in particular, phase composition and the relative cell edge lengths (a, b and c) were obtained. An estimation of the crystal size values was obtained from Scherrer equation in agreement with the GSAS package procedure. The agreement factors ("R values"), R_p, wR_p, R_F^2 and χ^2,[37] were generally acceptable. A standard deviation of ±0.003 Å for the refined cell parameters was estimated in the experimental conditions used in this work. The obtained Debye Waller factors for the perovskite-type phases are in good agreement with the literature ones. Debye Waller factors of secondary phases were set to 0.025 (standard value).

Specific surface area and porosity were determined by studying the gas-volumetric N_2 uptake at N_2 boiling point (-196° C) using an ASAP2020 gas-volumetric apparatus by Micromeritics. BET model[39] was applied for specific surface area determination and BJH model[40] was applied to the desorption branch of the isotherms and used for porosity characterization. Sample analyses were performed after outgassing in vacuo (residual pressure ~10^{-2} mbar) for several hours at 200 °C in order to reach a good surface cleaning.

FTIR spectra in the range 4000–400 cm^{-1} were recorded on a Jasco FT-IR 5300 spectrophotometer at the resolution of 4 cm^{-1}, effectuating 100 scans for each spectrum. Self-supporting pellet were prepared by 1 mg of sample and 160 mg of KBr, pressing the powder at 2 ton and let the pellet equilibrating for 2 minutes.

The powder morphology was observed by (High-Resolution) Transmission Electron Microscopy (HR-TEM), performed on a JEOL JEM 3010UHR (300 kV) TEM fitted with a single crystal LaB_6 filament. Samples were dry-deposited on Cu "holey" carbon grids (200 mesh).

Thermo-gravimetric analyses (TGA) were conducted in TGA Pyris 1 of Perkin-Elmer Instruments (Waltham, MA, USA), sensitivity 0.1 µg, with nitrogen feed (35 ml/min), heating from 25 °C up to 800 °C at 15 °C/min rate. The measurements were performed in aluminum oxide sample holders. As-burned powders before and after sonication protocol were examined.

A BRANSON 2510 sonicator (40kHz) and a ALC PK 131 R centrifuge with thermostat were employed for 24 hours sonication treatment.

Zeta potential measurements were performed on a Zetasizer Nano ZS Malvern Instrument. The zeta potential values were measured using principles of laser doppler velocitometry and phase analysis light scattering (M3-PALS technique). All the suspensions were prepared with 3 mg of powder and 12 ml of ultrapure water obtained from a Millipore Milli-Q™ system (TOC = 6 ppb).

Photocatalytic tests

For the photocatalytic tests two substrates were selected: 4-methylphenol (4-MP, >99% Aldrich) and crystal violet (CV, ≥90%, Sigma-Aldrich). Aqueous suspensions of $LaFeO_3$ photocatalyst (1200 mg L^{-1}) and substrate (10 mg L^{-1}) were prepared with Milli-Q™ ultrapure water and stirred for 30 minutes in order to grant homogenization before irradiation. The photodegradation trials were performed by irradiating the suspensions (5 mL) in closed Pyrex® cells under continuous stirring. Solar radiation was simulated in Solarbox, (CO.FO. Megra, Mi), a system equipped with Xenon lamp (1500 W) and cut-off filter for wavelengths below 340 nm.

After irradiation, in order to remove the photocatalyst, the samples were centrifuged or filtered through cellulose acetate 0.45 µm pores diameters filter (Millipore).

Degradation of 4-MP was followed by High Performance Liquid Chromatography (HPLC), employing a Merck-Hitachi instrument, equipped with Lichrospher RP-C18 column (125 mm x 4 mm i.d., d.p. 5 µm, from Merck), Rheodyne injector, L-6200 pumps and UV-VIS Merck Hitachi L-4200 detector and D-7000 HPLC System Manager (HSM) software. 4-MP was eluted employing isocratic condition, water (70%) and acetonitrile (30%). The flow rate was 1.0 mL min^{-1} and the retention time was 5.0 minutes. The detector wavelength was 220 nm.

The CV photobleaching was followed by a double beam UV-visible spectrophotometer CARY 100 SCAN-VARIAN. A sample quartz cell of 1 cm path length was used. The maximum absorbance of CV is 585 nm.

Results and discussion

Behaviour of CVT230 as combustion fuel

Interesting information about the role of the fuel can be obtained following the combustion process by Temperature-Time profiles which are reported in Fig. 2. The combustion of $LaFeO_3$ prepared from CVT230 is not single step, since the process needs more time than processes with traditional fuels like citric acid. The T-time profile curves report the temperature perceived by the thermocouple inserted in the reaction medium during the heating and subsequent combustion. The study of the curves brings important information about the kinetics of the combustion process. If the combustion wave propagates through all the mass of the precursor gel in few seconds, as in the case of citric acid used as fuel the T-time profile shows an unique peak. If the combustion wave is blocked for some reason, as in the case of CVT230 used as combustion fuel, more than one T-time peak is present in the T-time profile. The mechanism is the following. The combustion of the CVT230 occurs in several subsequent steps, so the combustion can be completed in one region, whereas a new combustion takes place in another region after

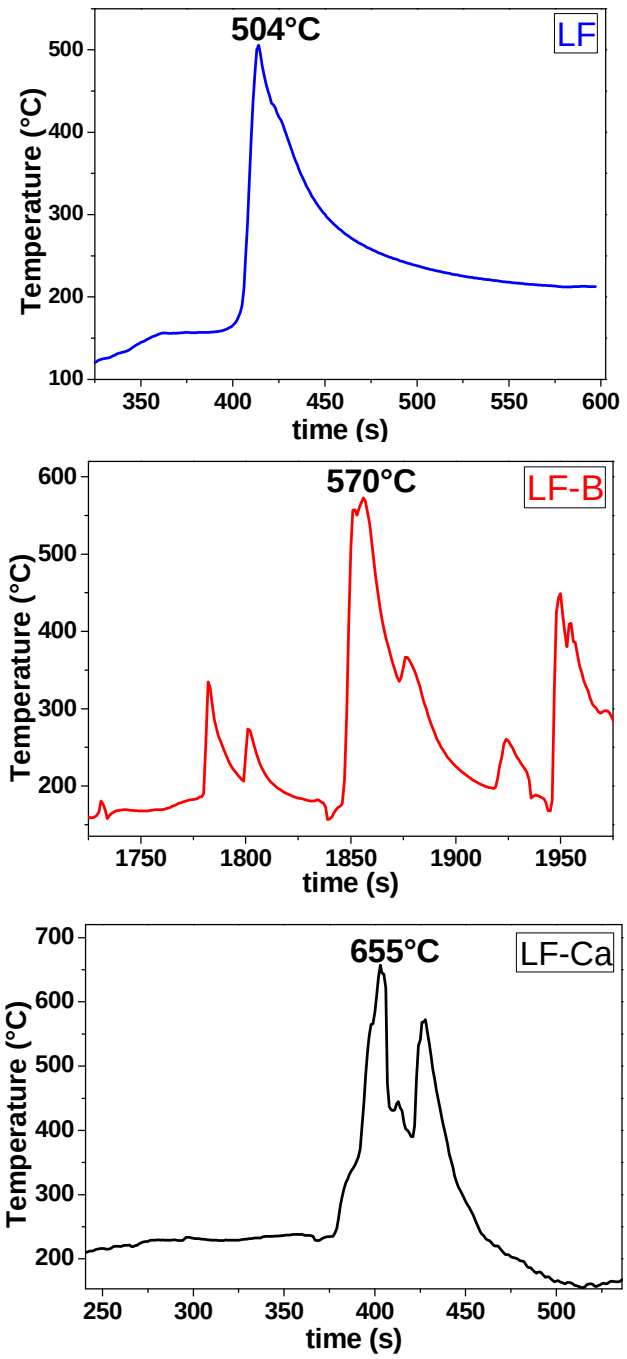

Fig. 2 Temperature-time profiles of the combustion process relative to LF, LF-B and LF-Ca samples.

some time. The thermocouple is in the center of the reaction beaker and perceives the high temperature combustion when the combustion occurs thereabout, whereas perceives other local combustion processes at lower temperatures when they occur away, depending on the position of the thermocouple with respect to the local combustion wave. When the gel mass has almost completely reacted, the gel has to be mixed manually in order to complete the process, until no more combustion waves are visible. A possible reason for this multistep decomposition might be the fact that SBO are mixture of different macromolecules[25] which might decompose in different conditions, causing a blocking of the combustion wave. Maximum temperature, initiation time and combustion intensity are also different for $LaFeO_3$ prepared from citric acid and from CVT230, consistently with the different nature of the fuels. LF-Ca sample, prepared from citric acid, is also reported in Fig.2 for comparison, since LF-B might contain as well some Ca, which is the major metal impurity coming from CVT230 (see table 1). The temperature-time profile is single step like for LF, although the maximum temperature and initiation temperatures are slightly higher than for LF. Moreover a double peak is evident in LF-Ca, like in the LF-B multiple peaks.

Furthermore, the T-time trend for the CVT230-derived sample suggests a not immediate transformation of precursors in final product, since the temperature continues to oscillate in a wide interval of time. In this condition, it is possible that precursors do not react completely and, moreover, remain entrapped in the forming $LaFeO_3$ structure. In order to evaluate this possibility, LF-B sample was submitted to sonication.

This treatment has been previously[41] proposed to favour the elimination of the templating agent from mesoporous materials. The material was then dried and physicochemically characterized. Fig. 3 shows the TGA profile of the samples as-burned and as-burned-sonicated.

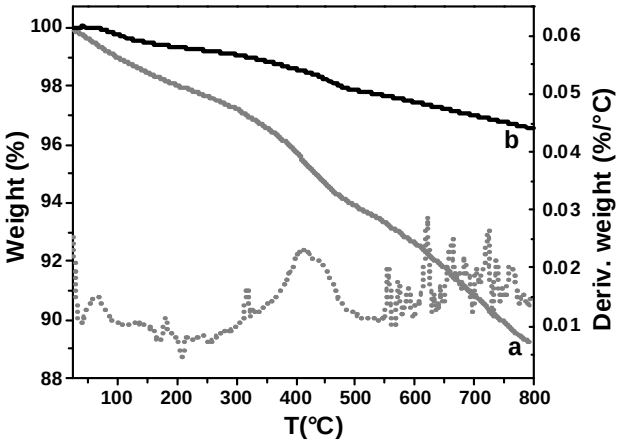

Fig 3. TGA curves obtained under nitrogen for: as-burned-sonicated sample (a), as-burned sample (b). Dotted line curve represents the derivative weight trend for as-burned-sonicated sample.

A continue weight loss is evidenced for the two samples, particularly evident for the as-burned-sonicated sample, with two important steps (more evident in the derivative dotted curve) are observable at about 100°C, and at temperatures higher than 400°C, representative of the elimination of adsorbed water and uncombusted organic matter. The as-burned sample (Fig. 3, curve b) shows a limited weight loss if compared with the as-burned-sonicated one, probably because the organic uncombusted residues left during the synthesis are present only on the sample surface. On the contrary, the as-burned-sonicated sample (Fig. 3, curve a) shows a larger amount of residues because the sonication treatment opens the closed porosities where the uncombusted precursors are trapped leaving them available for the decomposition in the TG experiments.

Fig. 4 shows the N_2 adsorption isotherms and pore size distribution for the LF-B samples, before and after sonication.

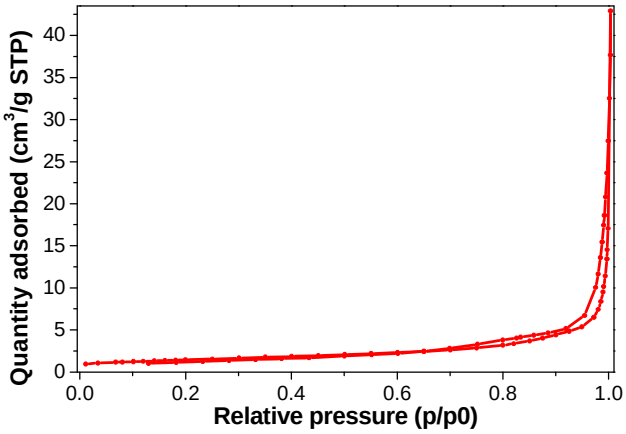

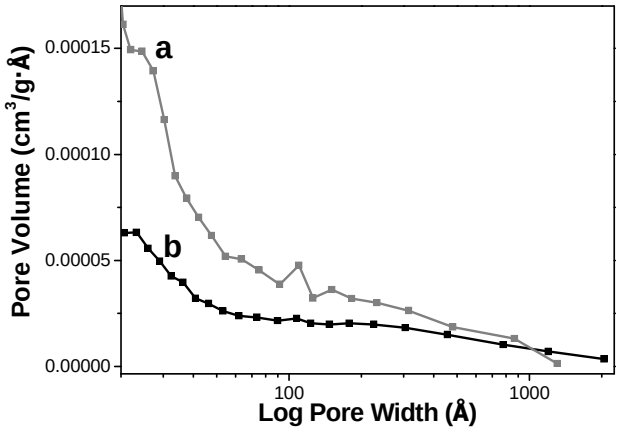

Fig. 4 N_2 adsorption isotherm for LF-B (calcined at 700°C for 5h) and pore size distributions for as-burned LF-B before (b) and after (a) sonication protocol.

Table 2 reports the BET specific surface areas and BJH total pore volumes for LF and LF-B recovered from the different treatments.

Table. 2 Surface values and total porosity of LF-B and LF after different treatments. These values are affected by a ±5% error.

Sample	*Surface area (m^2/g)*	*Total Porosity (cm^3/g)*
LF-B as-burned	5.0	0.03
LF-B as-burned and sonicated	21.0	0.08
LF-B calcined (700°C/5 h)	5.2	0.02
LF-B sonicated and calcined (700°C/5 h)	10.2	0.03
LF as-burned	17.0	0.08
LF as-burned and sonicated	22.0	0.11
LF calcined (700°C/5h)	11.0	0.06
LF sonicated and calcined (700°C/5h)	16.0	0.08

The adsorption isotherms of LF, LF-Ca and LF-B can be all classified as IV type (IUPAC classification), typical of mesoporous powders (see Fig.4a for LF-B). On the other hand,

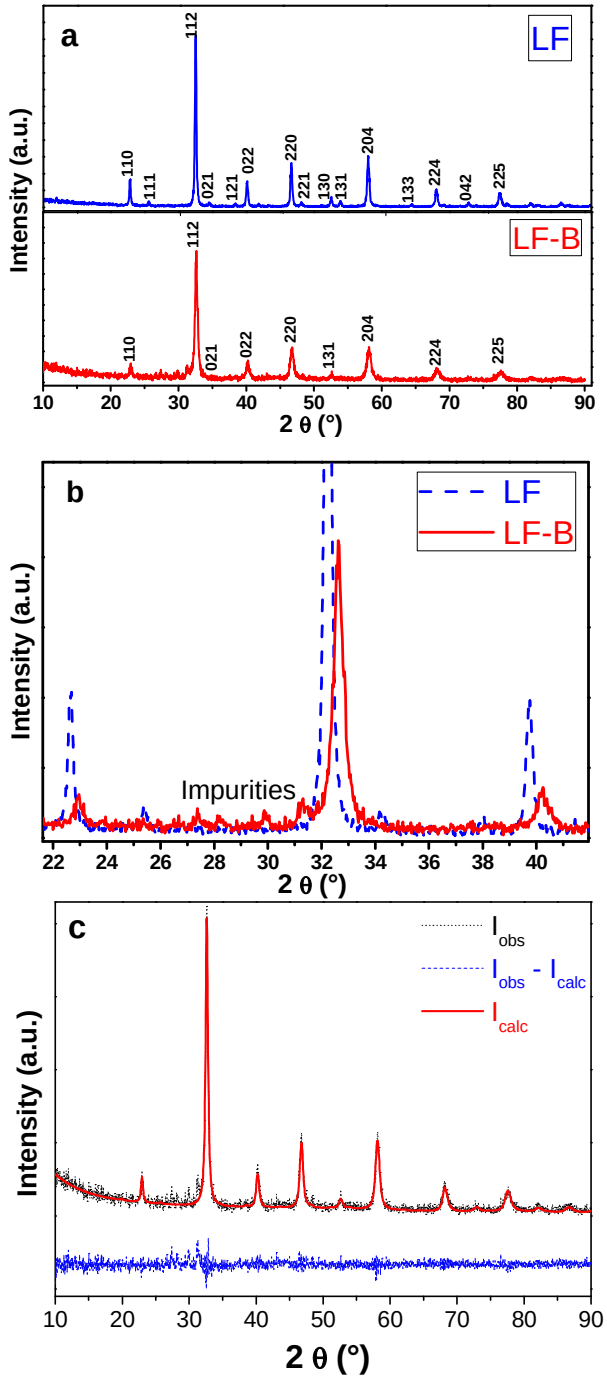

Fig. 5 Comparison between XRD patterns of a LF and LF-B, both calcined at 700°C/5 h. a) complete XRD pattern with miller indexes; b) details of the low angle region, where impurities and the difference in the peaks height and largeness are evident; c) Graphical Rietveld fit of LF-B after calcination at 700°C/5h. Impurities are not taken into account in the fitting procedure.

the adsorbed N_2 amount largely increases for sonicated samples (Table 2). Consequently, the BET surface area after sonication increases as well as the total porosity (Table 2). At the same time the pore size distribution curves indicate an increase of large pores which become visible and available to N_2 adsorption after the sonication treatment (Fig.4b). The larger porosity of the sonicated samples is maintained even after the thermal treatment

at 700°C, as showed in Table 2. Analogous results were evidenced for $LaFeO_3$ prepared by citric acid (Table 2) which were discussed in details in a previous paper.[42] In that case the effect was much less evident, in agreement with the different nature of the fuel.

Characterization of structure and morphology

XRD patterns of Fig. 5a, relative to calcined samples synthesized from citric acid and from CVT230, show essentially the same peaks, imputable to the $LaFeO_3$ phase (ICSD #164083). Nevertheless, there are some differences relative to intensity and shift of known peaks, as well as to the presence of peaks attributable to unidentified impurities (Fig.5b).

Peaks shift of Fig.5b indicates the presence of dopant cations in the perovskite structure. Metal cations other than La and Fe might come from inorganic residues present in the ashes of CVT230 (Table 1). Also EDX analyses (not shown), carried out on samples submitted to TEM investigation, confirmed the presence of impurities in the calcined LF-B materials. Among other possible doping species, calcium represents the most probable one, since it is the most abundant in the ashes (Table 1). Its effect on the perovskite is a cell volume contraction, as verified in XRD signals (Ca^{2+} is smaller than La^{3+}). Rietveld analysis was performed to obtain the cell parameters and to evaluate calcium amount in the $LaFeO_3$ structure. Fig. 5c shows the graphical Rietveld fit of LF-B as an example. Calculated cell parameters, crystal size and microstrain of LF-B, LF-Ca and LF are reported in Table 3, together with the reliability factors of the fit.

Table. 3. Structural parameters calculated from Rietveld analysis of the diffraction data.

	LF	LF-Ca	LF-B
***a* (Å)**	5.570	5.530	5.523
***b* (Å)**	7.859	7.808	7.811
***c* (Å)**	5.561	5.556	5.542
***Cell Volume* ($Å^3$)**	243.4	239.9	239.1
***Crystal Size* (nm)**	61	67	67
***Microstrain* (%)**	0.22	0.86	0.83
R_p (%)	14.1	15.6	16.0
wR_p (%)	21.5	22.4	22.6
R_F^2 (%)	11.7	14.8	16.5
χ^2	1.17	1.23	1.19

The data confirmed the cell volume contraction of LF-B (and LF-Ca) with respect to LF. Crystal size is nanometer-sized and for all the samples examined, a value of around 65 nm was calculated. Microstrain is smaller for LF than for the doped $LaFeO_3$ (LF-Ca and LF-B), in agreement with the larger strain caused by the replacement of trivalent dopants with divalent ones.

Taking the calculated LF and LF-Ca cell parameters as a reference, the calcium molar fraction of LF-B evaluated by Rietveld analysis is 0.25. On the other hand, the expected calcium molar fraction for LF-B, calculated from the CVT230 amount used in the syntheses and its ash content, is 0.37. It is evident that the calcium amount present in the contracted perovskite structure is much more limited than the calcium amount contributed from CVT230. It is possible that Ca excess accumulates outside the $LaFeO_3$ lattice as crystalline impurities detected by XRD or as amorphous species not detectable by XRD technique.

The calcined powders obtained from CVT230 and from citric acid have peculiar textural properties, which are mainly connected with the features assessed by CVT230 used as fuel.

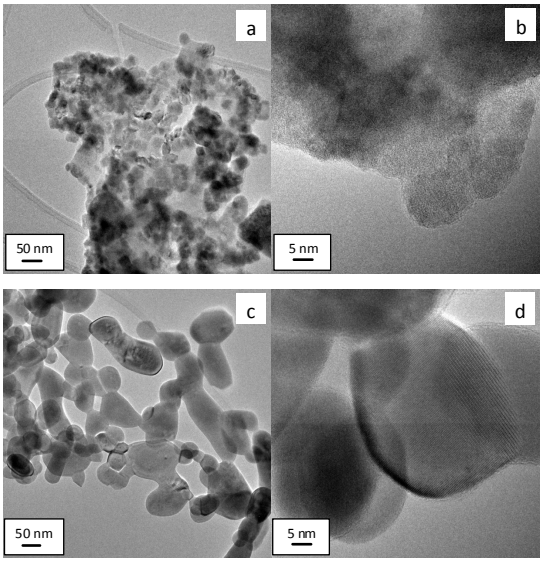

Fig. 6 TEM images (left sections: low magnification, right sections: high magnification).relative to LF-B (a) and LF (b) samples.

TEM images of Fig.6 report the comparison between LF-B and LF samples: LF-B particles (Fig.6a) have undefined shape, smaller size and a very close packing, as clearly visible in the high resolution image reported in Fig.6b. Otherwise, LF particles (Fig.6c and d) have roundish shape, larger size and a more limited aggregation.[42] No differences are evidenced by the analysis of the fringe patterns, which evidence the presence of $LaFeO_3$ phase. Although TEM observations confirm the nanometric size of both powders, already noticed by XRD analysis, it also evidence that the presence of CVT230 fuel seems to affect the size and regularity of the LF-B particles, which are smaller and thus more defective.

FT-IR measurements were performed on LF, LF-Ca and LF-B powders after calcination at 700°C/5h. Typical signals of the $LaFeO_3$ structure are visible in all the spectra reported in Fig. 7 (section A), confirming the presence of $LaFeO_3$ perovskite structure in all the examined powders. At the same time, a consistent presence of metal residues is suggested for LF-B by the occurrence of intense carbonate-like species bands (Fig.7-section B, C).

Indeed, the 585 cm^{-1} band in the LF-B spectrum of Fig.7 is attributable to the Fe-O antisymmetric stretching vibrations inside the octahedral structure FeO_6 (the shoulder at 619 cm^{-1} corresponds to symmetric stretching), while signals at 400 cm^{-1} are ascribable at O-Fe-O bending.[7,43,44] Splitting of ~400 cm^{-1}

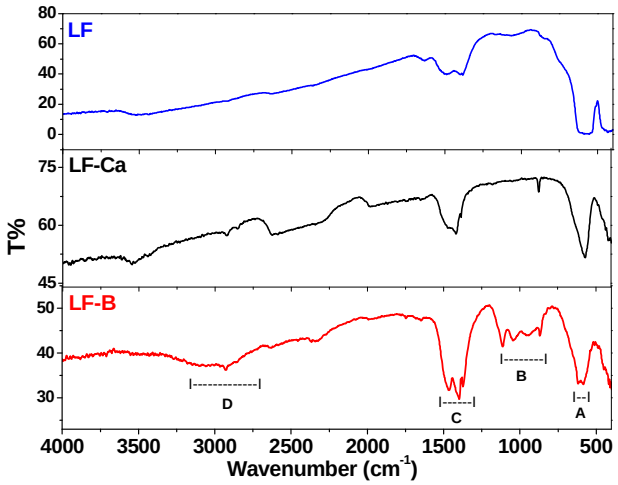

Fig. 7 FTIR absorption spectra of $LaFeO_3$ from citric acid (LF), Ca-doped $LaFeO_3$ from citric acid (LF-Ca) and $LaFeO_3$ from CVT230 (LF-B); A) Fe-O signals; B) carbonate ions and =CH signals; C) metal carbonates signals; D) CH signals.

band is caused by the structural deformation of the perovskite lattice with respect to the ideal cubic perovskite, in agreement with literature data.[45] Calcium is reported to be responsible of $LaFeO_3$ main peaks shift to higher frequencies. [43] However, in the present work no trend was found in the bands position upon increasing the amount of calcium in the sample.

Surface carbonate-like species, result of the interaction between atmospheric CO_2 and CVT230-derived materials, are identified at 869, 1046, 1466 and about 1400 cm^{-1} (Fig.7-sections B, C). Signals in the 1000-800 cm^{-1} range (section B) belong as well to the =CH bending of organic species derived from CVT230 decomposition, but can be also assigned to uncombusted CVT230 residues (C-O polysaccharide vibrations). LF and LF-Ca spectra are similar to the LF-B ones, although the signals of metal carbonates and organic species are less intense with respect to the LF-B signals. The weak peak at ~2350 cm^{-1} is imputable to CO_2 interacting with the material (adsorbed or entrapped), in agreement with the literature.[42] At about 3000 cm^{-1} (section D) CH stretching band is visible. OH signals are showed at high frequencies region, due to adsorbed H_2O or oxygenated organic residues, such as alcohols or phenols. Therefore, FT-IR characterization confirmed the presence of organic compounds and metal impurities in the CVT230-derived powder, in agreement with TGA, XRD and N_2-adsorption results.

Photocatalytic tests.

Aqueous suspensions of LF, LF-Ca and LF-B were tested for the degradation of two different substrates, 4-methylphenol (4-MP)and Crystal Violet (CV). The optimum concentration of catalyst to be employed in the experiments was preliminarily determined by irradiating for 3,5 hours different aqueous solutions of 4-MP (10 mg L^{-1}) in the presence of LF suspension in the concentration range 250-1500 mg L^{-1}. The degradation efficiency increased with LF concentration up to an upper limit of about 1200 mg L^{-1}. This concentration was therefore adopted for all the photocatalytic trials. The 4-MP substrate could be present in its negative ionized form depending on the operative pH values of the suspension, whereas CV is a cationic dye. They were chosen as model pollutants being able to show different charges in the adopted experimental conditions and to assess, if possible, the role played by electrostatic interaction and/or adsorption on the surface of the catalyst with respect to the photocatalytic probe molecule degradation.

Degradation of 4-MP

Fig.8 reports the data obtained using the three different materials differing for the reagents used in their preparation.

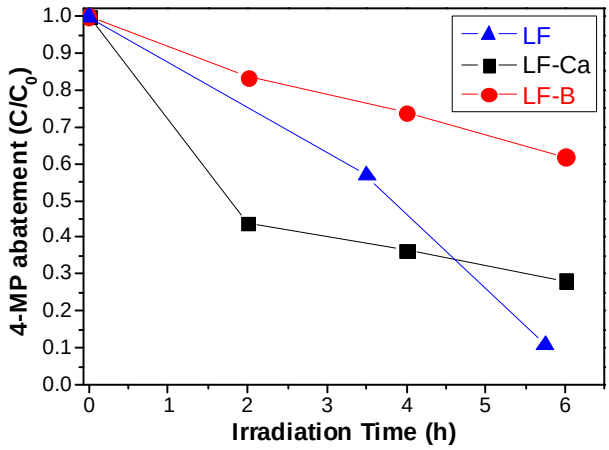

Fig.8: Abatement *vs* irradiation time for 10 mg L^{-1} 4-MP in the presence of 1200 mg L^{-1} LF, LF-Ca and LF-B. Abatement is expressed by C/C_0 ratio, where C_0 represents 4-MP concentration for not irradiated suspension.

In all cases, a progressive disappearance of 4-MP can be observed increasing the irradiation time. It clearly appears that after 6 hours of irradiation LF and LF-Ca perform significantly better than LF-B. In particular the most efficient behaviour is shown by LF. In the adopted experimental condition the operational pH was 8.0 for the LF and 10.0 for the LF-B photocatalyst suspensions. Under this condition, for the 4-MP, having a dissociation pK about 10, more than 90% of the substrate can be assumed in its undissociated form in the presence of LF whereas about 50% is present in the anionic form when using LF-B. At the same time LF particles possess a positive charge (based on the positive measured zeta potential value of +10.5). Beside the specific reactivity of 4-MP with the photogenerated active species[46] an interaction between the positively charged photocatalyst surface and the delocalized 4-MP aromatic electrons could not be ruled out in order to explain the results.

On the contrary, when working in the presence of LF-B a negative zeta potential of -22.1 was measured. In such conditions a possible repulsion between negatively charged surface particles and 4-MP in its dissociate form as well as aromatic electrons should be hypothesized; this phenomenon could contribute to explain the lower efficiency observed for LF-B.

CV photobleaching

When the CV solution undergoes irradiation in the presence of either LF or LF-B catalyst, a relevant different behaviour of the two systems was immediately evident by visual observation. In essence, it was observed only for the CV-LF-B suspension that,

upon filtration, the separated catalyst powder was strongly coloured This fact suggests that adsorption of the intensely coloured CV occurs only on the LF-B prepared material. Such behaviour is consistent with the negative measured zeta potential of the catalysts and the cationic nature of CV. In the experimental conditions applied an electrostatic attraction can take place between the cationic CV and the negatively charged LF-B surface. On the contrary, repulsion may occur between CV and the positively charged LF surface. After 6 hours of irradiation the complete colour abatement was observed in the presence of LF-B against a partial solution fading (about 30%) occurring in the presence of LF.

Conclusions

A $LaFeO_3$ heterogeneous photocatalyst was synthesized in the presence of a biowaste sourced soluble substance. With respect to ~~LF~~ the reference $LaFeO_3$ prepared from citric acid, this material shows different microstructural-textural properties and different photocatalytic activity for 4-methylphenol or Crystal Violet. In fact, the photocatalyst prepared in the presence of the biowaste sourced soluble substance was more effective in the removal of Crystal Violet from the solution. On the contrary, the citric acid-derived material catalyzed the photodegradation of 4-methylphenol more efficiently. These differences can be probably explained in terms of a different zeta potential on the surface, which is positively charged for the $LaFeO_3$ prepared from citric acid, but negatively charged for the samples prepared from the biowaste sourced soluble substance

Significant amount of entrapped matter was detected even in the calcined powders. This presence seems to be correlated to the Temperature-time profiles evidenced during the synthesis of materials, in particular in the presence of the biowaste sourced soluble substance, which causes a slow formation of the structure with the consequent entrapment of unreacted precursors in closed porosities. Although this might be viewed as a undesired phenomenon, a sonication treatment can be carried out to open the closed porosities increasing specific surface areas and porosity of the materials.

The results point out that the relative efficiency of $LaFeO_3$ photocatalysts synthesized using different reagents is strictly related to the target substrates to be degraded. A remarkable efficiency has been obtained for the LF-B obtained through sustainable processes, owing to the availability of cost-effective and environmentally compatible substances isolated from urban biowastes. To get deeper insight the degradation mechanism in order to optimize it, further investigation on photocatalysts synthesis in the presence of biowaste sourced soluble substances of different origin and chemical compositions seems worth to be pursued. As an additional point, it is possible to carry out an evaluation of the cost reduction, considering that the synthesis procedure was not greatly modified with respect to the classical one. Taking into account the cost of the fuels used, *i.e.*, bio-based surfactant *vs.* citric acid, the estimated cost for a bio-based surfactant, like the one used in this work is around 0.1-0.5 euro/kg, whereas the cost of citric acid is at least 50 euro/kg. This point alone should justify the industrial development of bio-based substances for materials preparation.

Acknowledgements

The authors are thankful to 7thFP IRSES-2010-269128-EnvironBos Marie Curie Action. Dr. Francesco Giordano and Dr. Erika Amore are greatly acknowledged, respectively for the XRD measurements and for help in zeta potential measurements. The authors are also thankful to Acea Pinerolese Spa in Pinerolo (TO) for supplying the bio-based substances sourcing materials.

Notes and references

[a] *Istituto per lo Studio dei Materiali Nanostrutturati (ISMN) - Consiglio Nazionale delle Ricerche (CNR), UOS Palermo, Via Ugo La Malfa 153, 90146, Palermo, Italy. Fax: +39 091 6809399; Tel: +39 091 6809387; E-mails: francesca.deganello@cnr.it; marialaura.tummino@pa.ismn.cnr.it; marialuisa.testa@cnr.it;carla.calabrese@studenti.unipa.it.*

[b] *Università di Torino, Dipartimento di Chimica, Via P. Giuria 7, 10125 Torino, Italy. Fax: +39 011 6705242; Tel: +39 011 6707631; E-mails: marialaura.tummino@unito.it; paola.avetta@unito.it; debora.fabbri@unito.it; alessandra.biancoprevot@unito.it; giuliana.magnacca@unito.it.*

[c] *Università di Foggia, STAR*Integrated Research Unit, Via Gramsci, 89-91, Foggia, Italy. E-mail: enzo.montoneri@gmail.com.*

[d] *NIS Centre of Excellence, Via P. Giuria 7, 10125 Torino, Italy. Fax: +39 011 670 7543; Tel: +39 011 670 7855; E-mail: giuliana.magnacca@unito.it.*

[*] *Corresponding author. email address.: francesca.deganello@cnr.it; telephone number.: +39-091-6809387; fax number.: +39-091-6809399.*

1 P.T. Anastas, J.B. Zimmerman, *Environ. Sci. Technol.*, 2003, **37**, 94A;
2 A. Kelarakis, *Adv. Mat. Lett.*, 2014, **5**, 236;
3 S. Thirumalairajan, K. Girija, N.Y. Hebalkar, D. Mangalaraj, C. Viswanathana, N. Ponpandian, *RSC Adv.*, 2013, **3**, 7549;
4 P.V. Gosavi, R. B. Bini, *Mat. Chem. Phys.*, 2010, **119**, 324;
5 R. Hu, C. Li, X. Wang, Y. Sun, H. Jia, H. Su, Y. Zhang, *Catal. Commun.*, 2012, **29**, 35;
6 F. Li, Y. Liu, R.H. Liu, Z. M. Sun, D. S. Zhao, C.G. Kou, *Mater. Lett.*, 2010, **64**, 223;
7 S. Li, L. Jing, W. Fu, L. Yang, B. Xin, H. Fu, *Mater. Res. Bull.*, 2007, **42**, 203;
8 J. Ding, X. Lü, H. Shu, J. Xie, H. Zhang, *Mater. Sci. Eng.*, 2010, **B 171**, 31;
9 H. Su, L. Jing, K. Shi, C. Yao, H. Fu, *J. Nanopart. Res*, 2010, **12**, 967;
10 V. Augugliaro, M. Litter, L. Palmisano, J. Soria, *J. Photochem. Photobiol. C, Photochem. Rev.*, 2006, **7**, 127;
11 M. Horáková, Š. Klementová, P. Kříž, S.K. Balakrishna, P. Špatenka, O. Golovko, P. Hájková, P. Exnar, *Surf. Coat. Tech.* 2014, **241**, 154;
12 M. Pera-Titus, V. García-Molina, M.A. Baños, J. Giménez, S. Esplugas, *Appl. Cat. B: Environ.*, 2004, **47**, 219;
13 A. Rubio-Clemente, R.A. Torres-Palma, G.A. Peñuela, *Sci. Total Environ.*, 2014, **478**, 201;
14 U.I. Gaya, A.H. Abdullah, *J. Photoch. Photobio. C: Photochem. Rev.*, 2008, **9**, 1;
15 S.Y. Lee, S.J. Park, *J. Ind. Engin. Chem.*, 2013, **19**, 1761;
16 T. Asada, T. Kayama, H. Kusaba, H. Einaga, Y. Teraoka, *Catalysis Today*, 2008, **139**, 37;
17 P. Xiao, J. Hong, T. Wang, X. Xu,Y. Yuan, J. Li, J. Zhu, *Catal. Lett.*, 2013, **143**, 887;
18 S.N. Tijare, M.V. Joshi, P.S. Padole, P.A. Mangrulkar, S.S. Rayalu, N.K. Labhsetwar, *Int. J. Hydrogen Energ.*, 2012, **10**, 10451;
19 R. Abazari, S. Sanati, *Superlatt. Microstr.*, 2013, **64**, 148;
20 O. Mihai, S. Raaen, D. Chen, A. Holmen, *J. Mater. Chem. A*, 2013, **1**, 7006;
21 S. Thirumalairajan, K. Girija, V. Ganesh, D. Mangalaraj, C. Viswanathan, N. Ponpandian, *Cryst. Growth Des.*, 2013, **13**, 291;
22 Z. Yang, Y. Huang, B. Dong, H. L. Li, *Materials Research Bulletin*, 2006, **41**, 274;

23 M. Ali Haider, A. J. Capizzi, M. Murayama, S. McIntosh, *Solid State Ionics*, 2011, **196**, 65;
24 K. Zhao, F. He, Z. Huang, A. Zheng, H. Li, Z. Zhao, *Int. J. Hydrogen Energ.*, 2014, **39**, 3243;
25 E. Montoneri, V. Boffa, P. Savarino, D. G. Perrone, C. Montoneri, R. Mendichi, E. J. Acosta, S. Kiran, *Biomacromolecules*, 2010, **11**, 3036;
26 E. Montoneri, D. Mainero, V. Boffa, D. G. Perrone, C. Montoneri *Int. J. Global Environ. Issues*, 2011, **11**, 170;
27 E. Montoneri, L. Tomasso, N. Colajanni, I. Zelano, F. Alberi, G. Cossa, R. Barberis, *Int. J. Environ. Sci. Technol.*, 2014, **11**, 251;
28 D. F. Mercado, G. Magnacca, M. Malandrino, A. Rubert, E. Montoneri, L. Celi, A. Bianco Prevot and M. C. Gonzalez, *ACS Appl. Mater. Interfaces*, 2014, **6**, 3937
29 V. Boffa, D.G. Perrone, E. Montoneri, G. Magnacca, L. Bertinetti, L. Garlasco, R. Mendichi, *Chem. Sus. Chem.*, 2010, **3**, 445;
30 V. Boffa, D.G. Perrone, G. Magnacca, E. Montoneri, Role of a waste-derived polymeric biosurfactant in the sol-gel synthesis of nanocrystalline titanium dioxide, *Ceram. Int.*, ~~in press~~ 2014,**40**,12161;
31 A. Bianco Prevot, P. Avetta, D. Fabbri, E. Laurenti, T. Marchis, D. G. Perrone, E. Montoneri, V. Boffa, *Chem. Sus. Chem.*, 2011, **4**, 85;
32 P. Avetta, F. Bella, A. Bianco Prevot, E. Laurenti, E. Montoneri, A. Arques, L. Carlos, *ACS Sustainable Chem. Eng.*, 2013, **1**, 1545;
33 P. Avetta, A. Bianco Prevot, D. Fabbri, E. Montoneri, L. Tomasso, *Chemical Engin. J.*, 2012, **197**, 193;
34 G. Magnacca, A. Allera, E. Montoneri, L. Celi, D. E. Benito, L. G. Gagliardi, M. C. Gonzalez , D. O. Mártire, L. Carlos, *ACS Sustainable Chem. Eng*., 2014, **2**, 1518.
35 F. Deganello, G. Marcì and G. Deganello, *J. Eur. Ceram. Soc.*, 2009, **29**, 439;
36 E. Montoneri, V. Boffa, P. Savarino, D. Perrone, M. Ghezzo, C. Montoneri, R. Mendichi, *Waste Management*, 2011, **31**, 10;
37 L.B. McCusker, R.B. Von Dreele, D.E. Coxd, D. Louer, P. Scardi, Rietveld refinement guidelines. *J. Appl. Cryst.*, 1999, **32**, 36;
38 A.C. Larson, R.B. Von Dreele, *GSAS General Structure Analysis System, LANSCE,MS-H805*. Los Alamos National Laboratory, Los Alamos, NM 87545, USA, 1998;
39 S. Brunauer, P.H. Emmett, E. Teller, *J. Am. Chem. Soc.*, 1938, **60**, 309;
40 E.P. Barrett, L.G. Joyner, P.P. Halenda, *J. Am. Chem. Soc.*, 1951, **73**, 373;
41 S. Jabariyan, M.A. Zanjanchi, *Ultrason. Sonochem.*, 2012, **19**, 1087;
42 G. Magnacca, G. Spezzati, F. Deganello, M.L. Testa, *RCS Adv.*, 2013, **3,** 26352;
43 B.P. Barbero, J.A. Gamboa, L.E. Cadús, *Appl. Catal. B: Environ.*, 2006, **65**, 21;
44 T. Liu, Y. Xu, *Mater.s Chem. Phys.*, 2011, **129**, 1047;
45 R. Andoulsi, K. Horchani-Neifer, M. Ferid, *Ceramica*, 2012, **58**, 126;

50